

pubs.acs.org/NanoLett Letter

# Nanoheterogeneity of LiTFSI Solutions Transitions Close to a Surface and with Concentration

Mengwei Han, Ruixian Zhang, Andrew A. Gewirth,\* and Rosa M. Espinosa-Marzal\*



Cite This: Nano Lett. 2021, 21, 2304-2309



**ACCESS** 

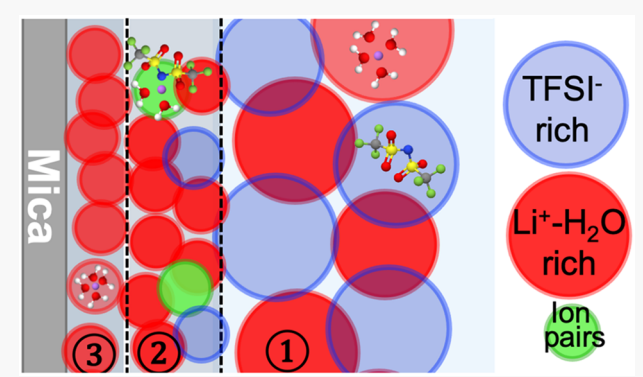
Metrics & More



Supporting Information

ABSTRACT: Water-in-salt (WIS) electrolytes composed of 21 *m* LiTFSI have recently emerged as a safe and environmentally friendly alternative to conventional organic electrolytes in Li-ion batteries. Several studies have emphasized the relation between the high conductivity of WIS electrolytes and their nanoscale structure. Combining force measurements with a surface forces apparatus and atomic force microscopy, this study describes the nanoheterogeneity of LiTFSI solutions as a function of concentration and distance from a negatively charged (mica) surface. We report various nanostructures coexisting in the WIS electrolyte, whose size increases with concentration and is influenced by the proximity of the mica surface. Two key concentration thresholds are identified, beyond which a transition of behavior is observed. The careful scrutinization on the concentration-dependent nanostructures lays groundwork for designing novel electrolytes in future energy storage devices.

KEYWORDS: Water-in-salt electrolytes, Surface forces, Nanostructures



# **■ INTRODUCTION**

Liquid electrolytes are ubiquitous in electrochemical systems including batteries, electrochemical actuators, and electrodeposition cells. A new paradigm of liquid electrolyte design has recently emerged. The idea is to reduce the solvent-to-ion ratio so that each ion is solvated by a very small number of solvent molecules, and counterions enter its solvation shell. Electrolytes have been engineered using this idea, under names including solvent-in-salt, solvent-limit, and superconcentrated electrolytes.

A water-in-salt (WIS) electrolyte composed of 21 m LiTFSI has been recently proposed to serve as a safe and environmentally benign alternative to traditional organic electrolytes. 7,8 When used in lithium-ion batteries, this WIS electrolyte enables high values of both the operating voltage and the cycling stability. While such high salt concentration typically impairs the electrolyte conductivity,<sup>9</sup> this electrolyte exhibits enhanced conductivity comparable to conventional nonaqueous electrolytes used in lithium-ion batteries. The merit has been ascribed to the formation of percolating nanodomains that are rich in either  $Li(H_2O)_4^+$  or  $[TFSI]^-$ , while the water-rich phase provides the enhanced mobility of the lithium cation. 10,11 The origin of this nanoscale heterogeneity is associated with the solvation disproportionation of Li<sup>+</sup> by water. In 21 m LiTFSI, 40% of Li<sup>+</sup> is solvated by only water, while 25% is solvated by only [TFSI]<sup>-,10</sup> and the inhomogeneous distribution of Li+ creates the two interpenetrating but dynamic networks. The TFSI-rich nanodomain relatively immobilizes the anion movement, while the [Li-(H<sub>2</sub>O)<sub>4</sub>]<sup>+</sup>-rich domain serves as a 3D percolating channel for fast Li<sup>+</sup> transport with high transference number, in contrast to the low transference numbers reported for dilute aqueous electrolytes. In addition, a host of interfacial processes such as the prevention of water electrosorption on cathodes and the formation of passivating solid electrolyte interphases (SEIs) on anodes are proposed to be responsible for the extraordinary performance of this WIS electrolyte. 12,7 Recently, we have reported the potential dependence of the interfacial structure of LiTFSI (21 m) on a gold surface. 13 Using AFM force measurements and surface-enhanced vibrational spectroscopy, it was concluded that the layers (0.64 and 0.67 nm) at positive potentials are associated with  $[Li(H_2O)_x]^+[TFSI^-]_v$  ion pairs, while the layers (0.28 and 0.33 nm) at negative potentials correspond to  $[Li(H_2O)_x]^+$  alone. This indicates that the interfacial structure deviates from the bulk nanoscale heterogeneity.

Received: January 14, 2021 Revised: February 12, 2021 Published: February 22, 2021





Despite these advances, the interfacial structure of this electrolyte still remains poorly understood. Using a surface forces apparatus (SFA) and atomic force microscopy, we reveal the transition of the WIS electrolyte nanostructure as a function of the distance from a negatively charged surface and the influence of concentration on such nanostructure. The advance in knowledge will be useful in further exploring the potential of utilizing concentrated electrolytes for energy storage devices.

# RESULTS

SFA measurements of the surface forces in LiTFSI solutions were carried out with nine different pairs of mica. The concentration of the LiTFSI solution was controlled in situ upon equilibration of the solution at constant relative humidity (RH) in the SFA fluid cell; see the Materials and Methods section in the Supporting Information. 21 m LiTFSI is in equilibrium with humid air at ~15% RH (Figure S1 in the SI). By increasing the humidity above 15% RH, water uptake occurs, and the concentration decreases. Most of the data were obtained between 22% and 55% RH, which corresponds to equilibrium concentrations between 18 and 8 m. SFA experiments were not possible for 21 m LiTFSI, because it led to crystallization between the mica surfaces. However, a few force curves were measured before the equilibration of the 21 m LiTFSI at 22% RH, while the concentration decreased from 21 to 18 m. Here, the precise value of the concentration is unknown, and the data are labeled as 18-21 m. The refractive index of the solution confined between the two mica surfaces was measured in films with a thickness of ~100 nm with our SFA. The observed increase of the refractive index from  $\sim$ 1.363 at 8 m, to 1.370 and 1.382 at 10 and 18 m, respectively, reflects the increase in concentration in the films confined between the surfaces upon equilibration at the selected RHs. Concurrently, the adhesive force between the mica surfaces increases from 0.5 to 5 and 15 mN/m with a decrease in concentration from 18 to 10 and 8 m, respectively (Figure S2), providing support to the idea that the increase in water content in the electrolyte promotes the wetting of the surface.

Figure 1a-d shows representative SFA results for the force between mica surfaces in LiTFSI solutions at concentrations of (a) 18 m, (b, c) 14 and 10 m, and (d) 8 m. The Figure shows the presence of a long-range repulsive force that decreases with surface separation (D > 10 nm). The decay is not clearly exponential, deviating from the characteristic behavior of dilute aqueous electrolytes, i.e., from an electrical double layer force. 14,15 The surface force in ionic liquids also follows a exponentially decaying profile 16 that differs from the behavior observed here. Such a repulsion between the two surfaces indicates the action of an osmotic pressure, which is sensed with our SFA at surface separations as large as ~88 nm. Figure S3 shows more measurements. We note that this long-range repulsive force shows significant variability at each concentration, and hence, a clear concentration dependence of the force is not found.

The surface force becomes more strongly repulsive as the surface separation decreases ( $D \lesssim 10$  nm); the characteristic decay length of this repulsion is  $1.69 \pm 0.27$  nm. Furthermore, there are multiple steps embedded on each force—separation curve, which indicates the superposition of an oscillatory force reflecting the presence of solvation layers that have a high affinity to the surface. These layers are composed of a molecular or supramolecular structural unit (e.g., hydrated ions

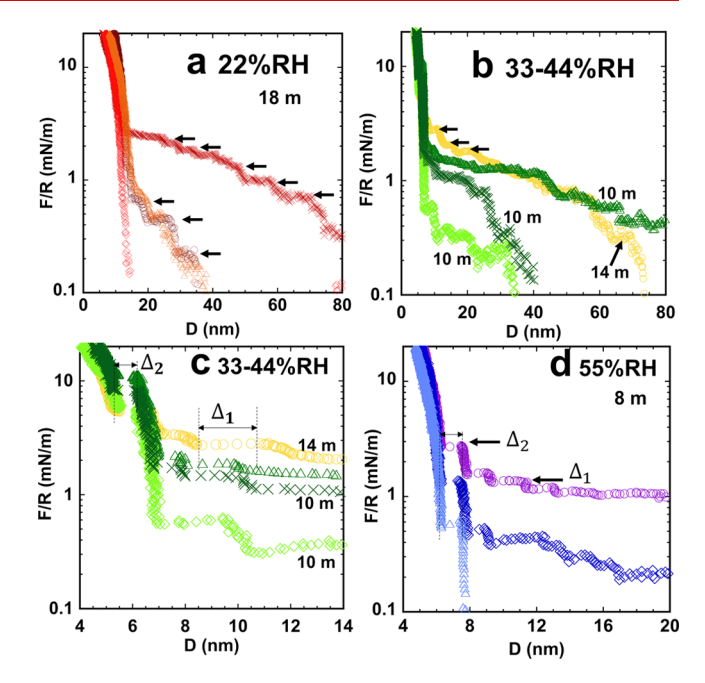
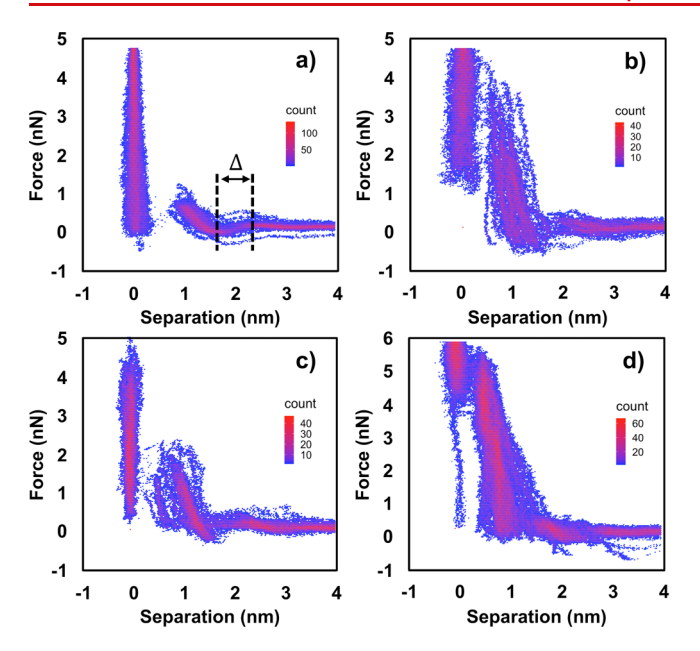


Figure 1. Representative surface forces between mica sheets in LiTFSI solutions measured with the SFA. (a, b) Long-range surface force in equilibrium with 22%, 33%, and 44% RH corresponding to 18, 14, and 10 m LiTFSI. Surface forces in equilibrium with 33%, 44%, and 55% RH (14, 10, and 8 m LiTFSI), at surface separations between (c) 4 and 14 nm and (d) 4 and 20 nm. The steps in the surface forces indicate the squeeze-out of layers composed of supramolecular structures (thickness  $\Delta_1$  and  $\Delta_2$ ) confined between the mica sheets. The color legend in this Letter is selected to be redorange for 22% RH (18 m), yellow for 33% RH (14 m), green for 44% RH (10 m), and blue for 55% RH (8 m).

or ion pairs). Steps in the short-range force have been reported for other solvents, including dilute aqueous electrolytes,  $^{17,18}$  ionic liquids,  $^{19-22}$  as well as water-in-ionic liquids.  $^{23,24}$  Figure 1a, however, reveals that the steps in the surface force extend to surface separations as large as  $\sim\!60$  nm. This behavior significantly deviates from the reported results for dilute electrolytes, where steps vanish at separations between mica surfaces  $D\gtrsim 3$  nm,  $^{18,25}$  and for most of the ionic liquids, but it is reminiscent of the behavior of liquid crystals, since they exhibit nanostructures that propagate over tens of nanometers from the surface.  $^{26,27}$ 

The magnitude of the force required to squeeze out surface-adsorbed layers has been related to the entropy of the confined structure and to the strength of the interaction between the molecules and the surface;  $^{15,28}$  a higher affinity of the molecules to the surface or a higher molecular ordering is associated with a higher force. Note that no interfacial layers were resolved at surface separation  $D\lesssim 2$  nm. This is likely because a force higher than that applied in these experiments (maximum  $\sim\!160$  mN/m) is required to squeeze out these molecules.

To determine the structure of the interfacial layers most strongly bound to mica (D < 4 nm), force measurements were carried out by AFM on freshly cleaved mica surfaces in LiTFSI solutions using a sharp silicon tip. The force—distance curves reveal 2–5 solvation layers at concentrations of 5, 10, 15, and 21 m, shown in Figure 2a–d, respectively, with characteristics that depend on concentration, as described later. In contrast, no solvation layers are resolved at 1 m (Figure S4a in the SI).



**Figure 2.** Heatmaps of force—distance curves measured by AFM on mica with a sharp silicon tip in (a) 5, (b) 10, (c) 15, and (d) 21 m LiTFSI solutions. The dashed line in part a) shows the definition of a layer, the size of which is denoted by  $\Delta$ . Each heat map was generated with 64 curves over an area of 500 nm by 500 nm. Figure S5 in the SI shows the superposed heatmaps.

The heatmaps at each concentration demonstrate the high reproducibility of the results on the mica surface over areas of  $500 \text{ nm} \times 500 \text{ nm}$ .

The thickness ( $\Delta$ ) of the solvation layers was determined as  $\Delta = D_i - D_j$  in SFA and AFM experiments, where  $D_i$  and  $D_j$  are the surface separation at which the squeeze-out event starts and ends, respectively ( $D_i > D_j$ ). Figure 3a shows the collection

of  $\Delta$  vs  $D_i$  inferred from SFA experiments. A transition of the layer thickness is observed, with smaller magnitude for smaller surface separations, except in 8 m LiTFSI. The colored lines help identify the transition from region 1 (at larger separations) to region 2 (at closer separations) for each concentration. Specifically, in 18 m LiTFSI,  $\Delta_2 \sim 0.99 \pm 0.10$ nm, while  $\Delta_1$  exhibits two plateaus, one at  $\Delta_1 \sim 1.80 \pm 0.20$ nm and a second one at  $\Delta_1 \sim 3.27 \pm 0.41$  nm (separately plotted in Figure 3b); a few values are larger than 4.00 nm, which correspond to the solutions with concentrations between 18 and 21 m. This is because some experiments were started prior to equilibration at 22% RH to examine a concentration closer to 21 m, before crystallization happened. At 14 m,  $\Delta_2 \sim 0.99 \pm 0.20$  nm, similar to that found in 18 m LiTFSI, but  $\Delta_1$  decreases to ~2.49  $\pm$  0.19 nm. Similarly, at 10 m,  $\Delta_2 \sim 0.81 \pm 0.08$  nm, while  $\Delta_1$  is reduced to  $\sim 1.93 \pm 0.12$ nm. In LiTFSI 8 m,  $\Delta_1$  exhibits a plateau at  $\sim$ 1.15  $\pm$  0.26 nm, while  $\Delta_2$  is larger (~1.58  $\pm$  0.16 nm) in this case, indicating a transition of the interfacial behavior with a decrease in concentration.

AFM experiments probe the interfacial structure closer to the surface (D < 4 nm, labeled as regions 2 and 3 in the inset of Figure 3a). At  $D \sim 1$  nm, the layer thickness appears to vary with concentration:  $\Delta_3 \sim 0.94 \pm 0.09$  nm for 5 m LiTFSI, while  $\Delta_3$  decreases to  $\sim 0.72 \pm 0.18$  nm, and  $\sim 0.79 \pm 0.20$  nm in 10 and 15 m LiTFSI, respectively. The larger standard deviation at these concentrations suggests certain variability in the layer thickness. At the highest concentration (21 m),  $\Delta_3$  decreases further to  $\sim 0.53 \pm 0.06$  nm, but a second (smaller) layer is resolved at higher forces  $\sim 0.25 \pm 0.14$  nm. In contrast, in region 2 ( $D \sim 1-4$  nm),  $\Delta_2$  is in the range 0.77–0.87 nm, and there is no clear concentration dependence. Note that we have labeled the spatial region located between 1 (probed by SFA) and 3 (probed by AFM, D < 1 nm) as region 2. The magnitude of  $\Delta_2$  measured by AFM is a bit smaller than that

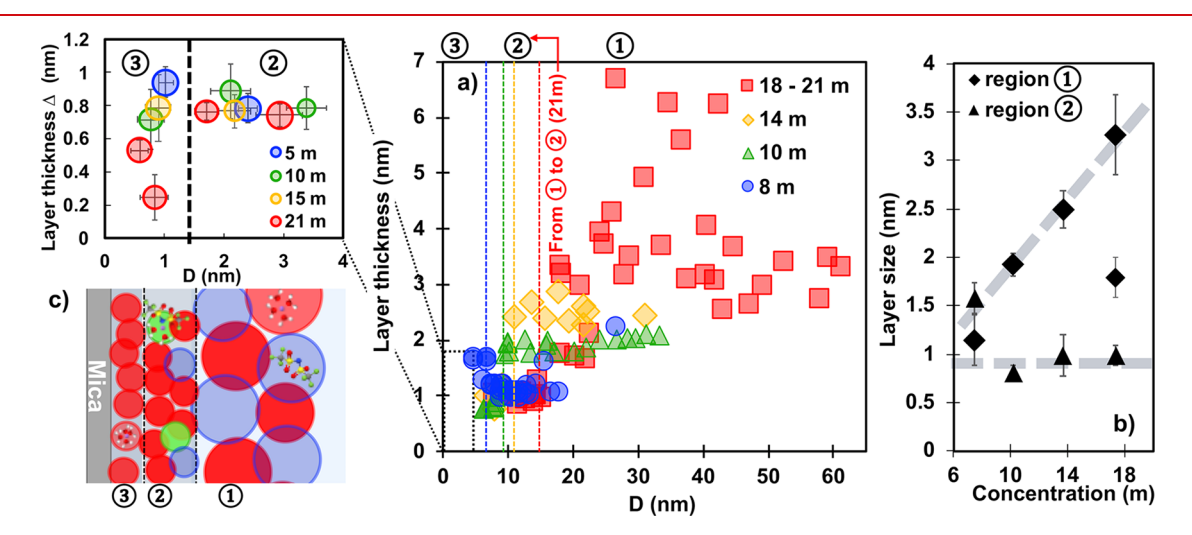


Figure 3. (a) Collection of layer thickness ( $\Delta$ ) vs surface separation (D) as resolved by SFA in the electrolyte solutions with concentrations of 8, 10, 14, and 18 m; some data correspond likely to higher but unknown concentrations, and hence, it is labeled as 18–21 m. The inset (top left) shows a bubble diagram with the layer thickness vs surface separation for D < 4 nm measured by AFM; the area of the bubbles represents the frequency of this layer size. Three regions are distinguished depending on the surface separation. The SFA probes regions 1 and 2. The colored dashed lines represent the transition between these two regions at each concentration: 8 m at  $D \sim 7$  nm (blue), 10 m at  $D \sim 10$  nm (green), 14 m at  $D \sim 11$  nm (yellow), and 18 m at  $D \sim 18$  nm (red, also labeled). The sharp tip probes regions 2 and 3 (D < 4 nm). (b)  $\Delta_1$  and  $\Delta_2$  (measured by SFA) as a function of concentration. The dashed lines are a guide to the eye. (c) Cartoon showing the hypothesized nanostructures in the three regions: In region  $\mathbb O$ , the nanoheterogeneity is composed of  $[\text{Li}(H_2O)_4]^+$ -rich (red) and  $[\text{TFSI}]^-$ -rich (blue) clusters, and it leads to layers of a few nm. In region  $\mathbb O$ , there is an excess of  $[\text{Li}(H_2O)_4]^+$  compared to TFSI anions near the mica surface and perhaps some ion pairs (green). In region  $\mathbb O$ , strongly adsorbed  $[\text{Li}(H_2O)_4]^+$  populates the interfacial region. The breakdown of this structure at 21 m LiTFSI is not shown.

measured by SFA (0.74–0.89 vs 0.80–0.99 nm) in the concentration range 10–21 m. However, considering the compressibility of the structural units, <sup>29</sup> and that the AFM tip pushes through the solvation layers at GPa pressure, while the solvation layers are squeezed out at MPa pressures by SFA, it is assumed that both instruments probe layers of a similar structure.

### DISCUSSION

The large size of the layers in region 1 indicates the presence of large nanostructures in the electrolyte. When measured by SFA, this implies that several structural units of similar size arrange parallel to the two surfaces, and this organization happens at surface separations as large as 60 nm. This longrange structure has not been observed in dilute electrolytes yet, and although it has been reported at least for an ionic liquid and for a water-in-ionic liquid,<sup>30,31</sup> it is not common in ionic liquids either. The SFA results in region 1 are reminiscent of the reported nanoheterogeneity of highly concentrated LiTFSI solutions based on spectroscopy, MD simulations, and small-angle neutron scattering.  $^{10,11}$  Our measurements show that  $\Delta_1$ increases monotonically with concentration (Figure 3b); it is  $1.15 \pm 0.26$ ,  $1.93 \pm 0.11$ , and  $2.49 \pm 0.19$  nm at 8, 10, and 14 m, respectively, while two plateaus are seen at 21 m, one at  $1.80 \pm 0.20$  nm and a second one at  $\sim 3.27 \pm 0.41$  nm. The length scale of Li-water clusters has been determined by MD simulations to lie between 1.0 and 2.0 nm at concentrations between 9 and 14 m. This length scale is in good agreement with our results in the same concentration range. 10 Simulations showed a subtle shift of the low-Q peak to a smaller Q-value (larger size) with increase in concentration, but the peak became less distinct, perhaps due to the broader size distribution observed in our experiments. Note that the presence of multiple layers over such large distances is only possible if both cation- and anion-rich domains are squeezed out to preserve electroneutrality. Therefore, we cannot exclude that strong correlations exist between Li-water clusters and anion-rich domains so that layers composed of several clusters are squeezed out during the approach of the surfaces. This could also justify the large magnitude of the layer thickness and standard deviation in 18 m LiTFSI. As mentioned earlier, the variability of the long-range surface force is much higher than in dilute electrolytes measured with the same instrument.<sup>25</sup> We believe that the long-range repulsion between the mica surfaces results from spatial density fluctuations stemming from the presence of these nanostructures. Each force measurement happens while the surfaces are slowly approaching, which could yield a different number of trapped structural units between the mica surfaces, and thereby an osmotic pressure of high variability.

The results for 8 m LiTFSI are intriguingly different. Not only is  $\Delta_2 = 1.58 \pm 0.16$  nm significantly larger than at higher concentrations, but also  $\Delta_1 = 1.15 \pm 0.26$  nm is much smaller, and no solvation layers are resolved at surface separations larger than 18 nm. The latter suggests that the structure of LiTFSI solutions at 8 m is much less prominent than at higher concentrations. This is consistent with prior MD simulations and neutron scattering experiments, which found that the liquid structure fully vanished at 5 m. Our measurements do not reveal the composition of these structural units, but we hypothesize that Li-water-rich clusters are still present in solution, perhaps a smaller number density, and the decreasing size with increasing distance from the surface indicates that

they start to vanish, thereby indicating a transition of behavior around this threshold concentration. It is possible that the higher water content closer to the mica surface explains why the clusters swell for 8 m LiTFSI so that  $\Delta_2 > \Delta_1$ , but this requires more investigation.

At such large distances, the effect of confinement is probably small, so that the observed nanostructure in region 1 is assumed to represent the nanoheterogeneity of the bulk electrolytes. In comparison, the nanostructure is expected to be more influenced by the proximity of the surface in regions 2 and 3. In 21 m LiTFSI, the interfacial structure closest to mica  $(\Delta_3 \sim 2.5 \text{ and } 0.53 \text{ nm, total } \sim 0.78 \text{ nm})$  deviates from the results at lower concentrations, representing another concentration threshold for the transition of the interfacial structure. In our previous work, 13 we combined surface-enhanced spectroscopy and AFM force measurements to elucidate the interfacial structure of 21 m LiTFSI on a smooth gold electrode. Two layers were resolved at negative bias potentials corresponding to  $[Li(H_2O)_x]^+$  alone, while at positive bias, the two layers were associated with  $[Li(H_2O)_x]^+$  ([TFSI]<sup>-</sup>)<sub>v</sub> ion pairs with excess negative charge. Hence, we believe that water and clusters rich in  $[Li(H_2O)_x]^+$  accumulate on the mica surface to counterbalance the negative charge. The larger layer thickness at concentrations smaller than 21 m ( $\Delta_3 \sim 0.95 \pm$ 0.07, 0.72  $\pm$  0.19, and 0.79  $\pm$  0.20 nm at 5, 10, and 15 m, respectively) could be justified by the higher water content; however, we cannot exclude that  $[Li(H_2O)_x]^+[TFSI]^-$  ion pairs are also present due to strong cation-anion correlations, especially with an increase in concentration. In 21 m LiTFSI, the breakdown of the nanostructure into two layers might originate from the decrease in water content and the high hydrophilicity of the mica surface, which outcompetes the Liwater clusters. In fact,  $\Delta_3 \sim 0.25$  and 0.53 nm agrees well with the diameter of a single water molecule and of the first hydration shell of Li<sup>+</sup> with 4 water molecules, <sup>10</sup> respectively. The magnitude of  $\Delta_3$  is close to  $\Delta_2$ , and hence, it is assumed that the composition of the layers in regions 2 and 3 is similar, except in the case of 21 m, where the breakdown of the nanostructure is proposed to happen on the mica surface. Note that decreasing the concentration to 5 and 8 m does not cause major deviations, which suggests that the mica surface plays a key role in determining the interfacial structure. Figure 3c presents an illustration of the proposed interfacial structure.

The nanoheterogeneity of highly concentrated LiTFSI electrolytes has been proposed to be responsible for its high conductivity. Our study suggests that the nanostructure changes in the proximity of the surface, and hence, it is reasonable that the conductivity in narrow cavities of nanometer size differs greatly from the bulk conductivity. We recognize that the properties of the electrode surface or of the SEI<sup>32,33</sup> differ from mica and will influence the interfacial structure in regions 1 and perhaps 2. Based on our results on mica and gold surfaces, <sup>13</sup> a change of interfacial composition at positive bias potentials or charge is expected, and the higher hydrophobicity of SEI could lead to a smaller hydration shell of  $[Li(H_2O)_x]^+$  close to the surface. The effect of the surface roughness has not been investigated yet, but striking results were reported for ionic liquids (ILs). MD simulations<sup>34</sup> suggested that roughness leads to a decrease in the charge ordering of ILs, while other simulations<sup>35</sup> showed that the presence of periodic ridges and valleys caused an increase in ordering; our AFM experiments showed that, for an IL on a nanorough silica surface, the interfacial layers prevailed but

were more disordered.<sup>36,37</sup> Understanding the effects of surface properties on the interfacial structure of WIS electrolytes is certainly of interest and requires future investigation.

# CONCLUSION

In summary, SFA and AFM force measurements in highly concentrated LiTFSI aqueous solutions reveal a prominent nanostructure that is disturbed by the proximity of the hydrophilic and negatively charged mica surface and is dependent on concentration. We distinguish three spatial regions to describe the resolved nanostructure. At concentrations exceeding 8 m, large structural units of nanometer length scale exist at separations between the mica surfaces larger than ~10 nm, (long-range structure), consistent with prior neutron scattering and MD simulations of the bulk electrolyte. We show, however, that their size increases monotonically with concentration ( $\Delta_1 = 1.0-6.0$  nm). Closer to the surface, the structural size is smaller and less dependent on concentration ( $\Delta_2 \sim 0.80-0.99$  nm), revealing the significant influence of the surface on the nanostructure. The structural units strongly bound to the surface, and therefore expected to be rich in Li<sup>+</sup>, are similar in size ( $\Delta_3 \sim 0.72-0.79$ nm), except at 21 m, where they break down in two distinct and smaller layers. This is likely due to the high hydrophilicity of the mica competing for the decreased water content in the solution. The long-range behavior is quite different at the concentration of 8 m. Here, the less prominent long-range structure is a footprint of the vanishing nanostructure of the bulk electrolyte. These results are consistent with prior studies of the nanoheterogeneity of water-in-salt LiTFSI electrolytes but extend the knowledge to the influence of a negatively charged surface and of the electrolyte concentration.

# ASSOCIATED CONTENT

# **Solution** Supporting Information

Materials and Methods; Figure S1. . The Supporting Information is available free of charge at https://pubs.acs.org/doi/10.1021/acs.nanolett.1c00167.

Materials and Methods, concentration of LiTFSI aqueous solution equilibrated at the range of relative humidity in this study and the water uptake kinetics, adhesion measured by SFA at different concentrations, example force—separation curves from SF, Force—separation curves measured in 1 *m* LiTFSI solution by AFM, and superposed heatmaps of force—separation curves measured by AFM (PDF)

# AUTHOR INFORMATION

### **Corresponding Authors**

Andrew A. Gewirth — Department of Chemistry, University of Illinois at Urbana—Champaign, Urbana, Illinois 61801, United States; oorcid.org/0000-0003-4400-9907; Email: agewirth@illinois.edu

Rosa M. Espinosa-Marzal — Department of Civil and Environmental Engineering and Department of Materials Science and Engineering, University of Illinois at Urbana—Champaign, Urbana, Illinois 61801, United States; orcid.org/0000-0003-3442-2511; Phone: +1-217-300-4380; Email: rosae@illinois.edu

#### **Authors**

Mengwei Han – Department of Civil and Environmental Engineering, University of Illinois at Urbana–Champaign, Urbana, Illinois 61801, United States

Ruixian Zhang — Department of Chemistry, University of Illinois at Urbana—Champaign, Urbana, Illinois 61801, United States

Complete contact information is available at: https://pubs.acs.org/10.1021/acs.nanolett.1c00167

#### **Author Contributions**

The manuscript was written through contributions of all authors. All authors have given approval to the final version of the manuscript.

#### **Funding**

This work was supported by the National Science Foundation Grant NSF DMR 19-04681 (to R.M.E.-M.) and as part of the Joint Center for Energy Storage Research (JCESR), an Energy Innovation Hub funded by the U.S. Department of Energy, Office of Science, Basic Energy Sciences (to A.A.G.).

#### Notes

The authors declare no competing financial interest.

#### REFERENCES

- (1) Azov, V. A.; Egorova, K. S.; Seitkalieva, M. M.; Kashin, A. S.; Ananikov, V. P. Solvent-in-salt" systems for design of new materials in chemistry, biology and energy research. *Chem. Soc. Rev.* **2018**, *47* (4), 1250–1284.
- (2) Yamada, Y.; Yamada, A. Superconcentrated Electrolytes to Create New Interfacial Chemistry in Non-aqueous and Aqueous Rechargeable Batteries. *Chem. Lett.* **2017**, *46* (8), 1056–1064.
- (3) Yamada, Y.; Wang, J.; Ko, S.; Watanabe, E.; Yamada, A. Advances and issues in developing salt-concentrated battery electrolytes. *Nat. Energy* **2019**, *4* (4), 269–280.
- (4) Zheng, J.; Lochala, J. A.; Kwok, A.; Deng, Z. D.; Xiao, J. Research Progress towards Understanding the Unique Interfaces between Concentrated Electrolytes and Electrodes for Energy Storage Applications. *Adv. Sci. (Weinh)* **2017**, *4* (8), 1700032.
- (5) Zhang, S.; Sun, J.; Zhang, X.; Xin, J.; Miao, Q.; Wang, J. Ionic liquid-based green processes for energy production. *Chem. Soc. Rev.* **2014**, *43* (22), 7838–69.
- (6) Zhong, C.; Deng, Y.; Hu, W.; Qiao, J.; Zhang, L.; Zhang, J. A review of electrolyte materials and compositions for electrochemical supercapacitors. *Chem. Soc. Rev.* **2015**, 44 (21), 7484–539.
- (7) Suo, L.; Borodin, O.; Gao, T.; Olguin, M.; Ho, J.; Fan, X.; Luo, C.; Wang, C.; Xu, K. Water-in-salt" electrolyte enables high-voltage aqueous lithium-ion chemistries. *Science* **2015**, *350* (6263), 938–943.
- (8) Suo, L.; Han, F.; Fan, X.; Liu, H.; Xu, K.; Wang, C. Water-in-Salt" electrolytes enable green and safe Li-ion batteries for large scale electric energy storage applications. *J. Mater. Chem. A* **2016**, *4* (17), 6639–6644.
- (9) Xu, K. Nonaqueous Liquid Electrolytes for Lithium-Based Rechargeable Batteries. Chem. Rev. 2004, 104 (10), 4303–4418.
- (10) Borodin, O.; Suo, L.; Gobet, M.; Ren, X.; Wang, F.; Faraone, A.; Peng, J.; Olguin, M.; Schroeder, M.; Ding, M. S.; Gobrogge, E.; von Wald Cresce, A.; Munoz, S.; Dura, J. A.; Greenbaum, S.; Wang, C.; Xu, K. Liquid Structure with Nano-Heterogeneity Promotes Cationic Transport in Concentrated Electrolytes. *ACS Nano* **2017**, *11* (10), 10462–10471.
- (11) Lim, J.; Park, K.; Lee, H.; Kim, J.; Kwak, K.; Cho, M. Nanometric Water Channels in Water-in-Salt Lithium Ion Battery Electrolyte. J. Am. Chem. Soc. 2018, 140 (46), 15661–15667.
- (12) McEldrew, M.; Goodwin, Z. A. H.; Kornyshev, A. A.; Bazant, M. Z. Theory of the Double Layer in Water-in-Salt Electrolytes. *J. Phys. Chem. Lett.* **2018**, *9*, 5840–5846.

- (13) Zhang, R.; Han, M.; Ta, K.; Madsen, K. E.; Chen, X.; Zhang, X.; Espinosa-Marzal, R. M.; Gewirth, A. A. Potential-Dependent Layering in the Electrochemical Double Layer of Water-in-Salt Electrolytes. ACS Appl. Energy Mater. 2020, 3 (8), 8086–8094.
- (14) Adamson, A. W.; Gast, A. P. Physical chemistry of surfaces; Interscience publishers: New York, 1967; Vol. 150.
- (15) Israelachvili, J. N. Intermolecular and surface forces, 3rd ed.; Academic press: San Diego, 2011.
- (16) Gebbie, M. A.; Dobbs, H. A.; Valtiner, M.; Israelachvili, J. N. Long-range electrostatic screening in ionic liquids. *Proc. Natl. Acad. Sci. U. S. A.* **2015**, *112* (24), 7432–7437.
- (17) Israelachvili, J. N.; Pashley, R. M. Molecular layering of water at surfaces and origin of repulsive hydration forces. *Nature* **1983**, *306* (5940), 249–250.
- (18) Espinosa-Marzal, R. M.; Drobek, T.; Balmer, T.; Heuberger, M. P. Hydrated-ion ordering in electrical double layers. *Phys. Chem. Chem. Phys.* **2012**, *14* (17), 6085–6093.
- (19) Atkin, R.; Warr, G. G. Structure in Confined Room-Temperature Ionic Liquids. *J. Phys. Chem. C* **2007**, *111* (13), 5162–5168.
- (20) Perkin, S.; Albrecht, T.; Klein, J. Layering and shear properties of an ionic liquid, 1-ethyl-3-methylimidazolium ethylsulfate, confined to nano-films between mica surfaces. *Phys. Chem. Chem. Phys.* **2010**, 12 (6), 1243–7.
- (21) Espinosa-Marzal, R. M.; Arcifa, A.; Rossi, A.; Spencer, N. D. Microslips to "Avalanches" in Confined, Molecular Layers of Ionic Liquids. *J. Phys. Chem. Lett.* **2014**, *5* (1), 179–84.
- (22) Horn, R. G.; Evans, D. F.; Ninham, B. W. Double-layer and solvation forces measured in a molten salt and its mixtures with water. *J. Phys. Chem.* **1988**, *92* (12), 3531–3537.
- (23) Espinosa-Marzal, R. M.; Arcifa, A.; Rossi, A.; Spencer, N. D. Ionic Liquids Confined in Hydrophilic Nanocontacts: Structure and Lubricity in the Presence of Water. *J. Phys. Chem. C* **2014**, *118* (12), 6491–6503.
- (24) Han, M.; Espinosa-Marzal, R. M. Influence of Water on Structure, Dynamics, and Electrostatics of Hydrophilic and Hydrophobic Ionic Liquids in Charged and Hydrophilic Confinement between Mica Surfaces. ACS Appl. Mater. Interfaces 2019, 11 (36), 33465–33477.
- (25) Zachariah, Z.; Espinosa-Marzal, R. M.; Heuberger, M. P. Ion specific hydration in nano-confined electrical double layers. *J. Colloid Interface Sci.* **2017**, *506*, 263–270.
- (26) Ruths, M.; Granick, S. Influence of Alignment of Crystalline Confining Surfaces on Static Forces and Shear in a Liquid Crystal, 4'n-Pentyl-4-cyanobiphenyl. *Langmuir* **2000**, *16* (22), 8368–8376.
- (27) Ruths, M.; Steinberg, S.; Israelachvili, J. N. Effects of Confinement and Shear on the Properties of Thin Films of Thermotropic Liquid Crystal. *Langmuir* **1996**, *12* (26), 6637–6650.
- (28) Donaldson, S. H.; Røyne, A.; Kristiansen, K.; Rapp, M. V.; Das, S.; Gebbie, M. A.; Lee, D. W.; Stock, P.; Valtiner, M.; Israelachvili, J. Developing a General Interaction Potential for Hydrophobic and Hydrophilic Interactions. *Langmuir* **2015**, *31* (7), 2051–2064.
- (29) Lee, S. S.; Fenter, P.; Nagy, K. L.; Sturchio, N. C. Monovalent Ion Adsorption at the Muscovite (001)-Solution Interface: Relationships among Ion Coverage and Speciation, Interfacial Water Structure, and Substrate Relaxation. *Langmuir* **2012**, 28 (23), 8637–8650.
- (30) Jurado, L. A.; Kim, H.; Rossi, A.; Arcifa, A.; Schuh, J. K.; Spencer, N. D.; Leal, C.; Ewoldt, R. H.; Espinosa-Marzal, R. M. Effect of the environmental humidity on the bulk, interfacial and nanoconfined properties of an ionic liquid. *Phys. Chem. Chem. Phys.* **2016**, *18* (32), 22719–30.
- (31) Jurado, L. A.; Kim, H.; Arcifa, A.; Rossi, A.; Leal, C.; Spencer, N. D.; Espinosa-Marzal, R. M. Irreversible structural change of a dry ionic liquid under nanoconfinement. *Phys. Chem. Chem. Phys.* **2015**, 17 (20), 13613–24.
- (32) Yamada, Y.; Furukawa, K.; Sodeyama, K.; Kikuchi, K.; Yaegashi, M.; Tateyama, Y.; Yamada, A. Unusual Stability of Acetonitrile-Based

- Superconcentrated Electrolytes for Fast-Charging Lithium-Ion Batteries. J. Am. Chem. Soc. 2014, 136, 5039-5046.
- (33) Wang, F.; Borodin, O.; Ding, M. S.; Gobet, M.; Vatamanu, J.; Fan, X.; Gao, T.; Eidson, N.; Liang, Y.; Sun, W.; et al. Hybrid Aqueous/Non-aqueous Electrolyte for Safe and High-Energy Li-Ion Batteries. *Joule* **2018**, *2*, 927–937.
- (34) Mendonça, A. C. F.; Pádua, A. A. H.; Malfreyt, P. Nonequilibrium Molecular Simulations of New Ionic Lubricants at Metallic Surfaces: Prediction of the Friction. *J. Chem. Theory Comput.* **2013**, 9 (3), 1600–1610.
- (35) David, A.; Fajardo, O. Y.; Kornyshev, A. A.; Urbakh, M.; Bresme, F. Electrotunable lubricity with ionic liquids: the influence of nanoscale roughness. *Faraday Discuss.* **2017**, *199*, 279–297.
- (36) Nalam, P. C.; Sheehan, A.; Han, M.; Espinosa-Marzal, R. M. Effects of Nanoscale Roughness on the Lubricious Behavior of an Ionic Liquid. *Adv. Mater. Interfaces* **2020**, *7* (17), 2000314.
- (37) Sheehan, A.; Jurado, L. A.; Ramakrishna, S. N.; Arcifa, A.; Rossi, A.; Spencer, N. D.; Espinosa-Marzal, R. M. Layering of ionic liquids on rough surfaces. *Nanoscale* **2016**, 8 (7), 4094–4106.